

Sediment focusing creates 100-ka cycles in interplanetary dust accumulation on the Ontong Java Plateau

Sean M. Higgins^{a,*}, Robert F. Anderson^a, Franco Marcantonio^b,
Peter Schlosser^a, Martin Stute^{a,c}

^a Lamont-Doherty Earth Observatory of Columbia University, Palisades, NY 10964, USA

^b Department of Geology, Tulane University, New Orleans, LA 70118, USA

^c Department of Environmental Sciences, Barnard College, New York, NY 10027, USA

Received 21 January 2002; received in revised form 18 July 2002; accepted 24 July 2002

Abstract

The accumulation of extraterrestrial ^3He , a tracer for interplanetary dust particles (IDPs), in sediments from the Ontong Java Plateau (OJP; western equatorial Pacific Ocean) has been shown previously to exhibit a regular cyclicity during the late Pleistocene, with a period of ~ 100 ka. Those results have been interpreted to reflect periodic variability in the global accretion of IDPs that, in turn, has been linked to changes in the inclination of Earth's orbit with respect to the invariable plane of the solar system. Here we show that the accumulation in OJP sediments of authigenic ^{230}Th , produced by radioactive decay of ^{234}U in seawater, exhibits a 100-ka cyclicity similar in phase and amplitude to that evident in the ^3He record. We interpret the similar patterns of ^{230}Th and ^3He accumulation to reflect a common origin within the ocean–climate system. Comparing spatial and temporal patterns of sediment accumulation against regional patterns of biological productivity and against the well-established pattern of CaCO_3 dissolution in the deep Pacific Ocean leads to the further conclusion that a common 100-ka cycle in accumulation of biogenic, authigenic and extraterrestrial constituents in OJP sediments reflects the influence of climate-related changes in sediment focusing, rather than changes in the rate of production or supply of sedimentary constituents.

© 2002 Elsevier Science B.V. All rights reserved.

Keywords: cosmic dust; Th-230; sediment supply; Ontong Java Plateau; He-3

1. Introduction

The Milankovitch hypothesis that links regular

cycles of climate variability to subtle variations in Earth's orbit has gained widespread acceptance among paleoclimatologists [1–4]. A perplexing weakness of this theory, however, is that the forcing associated with the 100-ka eccentricity cycle in Earth's orbit seems to be too weak to account for the 100-ka cyclicity in global ice volume that has dominated late-Pleistocene climate [5,6]. Muller and MacDonald [7,8] proposed an alternative mechanism in which the 100-ka cycle of global

* Corresponding author. Present address: MIT, Department of Earth, Atmospheric, and Planetary Sciences, E34-172, 42–44 Carleton Street, Cambridge, MA 02139, USA.
Tel.: +1-617-258-5572; fax: +1-617-253-8630.

E-mail address: shiggins@mit.edu (S.M. Higgins).

ice volume is linked to changes in the inclination of Earth's orbit relative to the solar system invariable plane. One proposed consequence of this mechanism is that the flux of extraterrestrial material reaching the Earth would also vary with a 100-ka periodicity [9,10], allowing the hypothesis to be tested by reconstructing the flux of interplanetary dust particles (IDPs) over a period of sufficient duration to detect 100-ka cycles. A convenient geochemical proxy for IDPs is ^3He , which is present at high concentrations in these particles [11]. If the 100-ka cycle in inclination of Earth's orbit creates significant variability in the accretion of extraterrestrial material, then this should be apparent in records of extraterrestrial ^3He accumulation in marine sediments.

Approximately 30 000 tons of IDPs are deposited at the Earth's surface every year [11]. Only about 1% (or those IDPs $< 30 \mu\text{m}$) of the total IDP flux to Earth retains its solar wind-implanted He signature and it is this ^3He that serves as a proxy for past changes in IDP accretion [12]. The average size of these ^3He retentive IDPs has been estimated to be $\sim 10 \mu\text{m}$ or less. In deep-sea sediments, the extraterrestrial source dominates the total supply of ^3He . Corrections for the small contribution of ^3He from terrigenous sources can be made using appropriate values for the terrigenous $^3\text{He}/^4\text{He}$ ratio together with the measured ^3He and ^4He concentrations [13,14].

Following this approach, Farley and Patterson [13] reported a 100-ka cycle in the accumulation rate of extraterrestrial ^3He in North Atlantic sediments (Site ODP607) during the interval between 250 and 450 ka. Later, Patterson and Farley [15] found evidence for a 100-ka cycle in ^3He accumulation over the past 700 ka in sediments from the Ontong Java Plateau (OJP; Site ODP806) in the western equatorial Pacific Ocean. While the existence of a 100-ka cycle in ^3He accumulation appeared to support Muller's hypothesis ([7,8]; see above), some important concerns have been identified.

For example, Marcantonio et al. [16–18] found 100-ka cycles in IDP accumulation during the past 200–300 ka in four cores from the central equatorial Pacific Ocean. These cycles were eliminated when ^3He accumulation was re-evaluated

by normalizing to ^{230}Th [16,17], leading Marcantonio et al. to postulate that these features resulted from climate-related changes in sediment focusing (i.e. the focused deposition of sediment transported laterally by deep-sea currents), rather than from changes in the supply of IDPs from space. Subsequently, the study of 12 additional deep-sea cores from a variety of different sedimentary environments in the Atlantic, Pacific, and Indian oceans found no evidence for 100-ka cycles in ^{230}Th -normalized rates of ^3He accumulation over the past 300 ka [19].

Here, we re-examine the record of ^3He accumulation in OJP sediments by comparing concentrations and accumulation rates of ^3He to those of initial (decay-corrected) unsupported ^{230}Th ($x_s^{230}\text{Th}(o)$). Accumulation of $x_s^{230}\text{Th}(o)$ exhibits a 100-ka cycle nearly identical in phase and amplitude to that observed for ^3He , suggesting that the origin of these 100-ka cycles is internal to the ocean–climate system rather than involving changes in delivery of IDPs from space. The pattern of $x_s^{230}\text{Th}(o)$ accumulation is diagnostic of climate-related changes in sediment redistribution, which must have influenced the accumulation of IDPs as well.

2. Study area

The OJP has been an area of extensive paleoceanographic research. Because the plateau rises to depths as shallow as $\sim 1500 \text{m}$, CaCO_3 preservation there is better than throughout most of the deep Pacific Ocean. Consequently, sediments from the OJP have been studied extensively to reconstruct changes in ocean chemistry, productivity, and hydrography throughout the late Quaternary [20–24].

A study of Holocene OJP sediments by Broecker et al. [25] provides evidence for higher accumulation rates of carbonate and clays at the equator than off the equator. Subsequently, by measuring $x_s^{230}\text{Th}(o)$ and Al/Ti ratios in surface sediments at some of the sites studied by Broecker et al., Higgins et al. [26] concluded that sediment is focused into a narrow belt along the equatorial region of the OJP. Those results further indicated that the

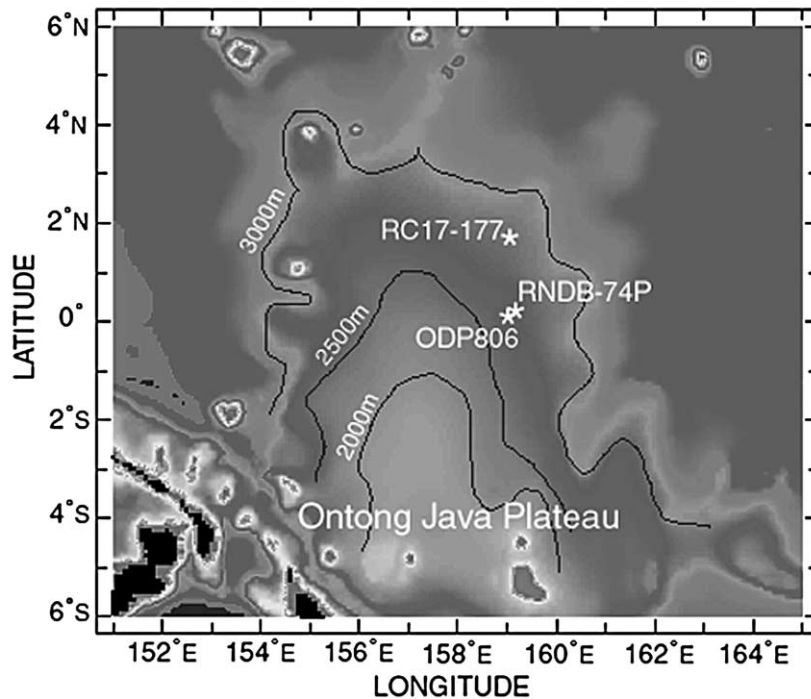


Fig. 1. Map of the Ontong Java Plateau showing locations where cores discussed in this paper were recovered. Isobaths at 2000 m, 2500 m and 3000 m are also shown.

detrital and biogenic fractions of the sediments, as well as the $x_s^{230}\text{Th}(o)$ derived from water column, have all been focused without detectable fractionation among the sedimentary constituents. On a longer timescale, Schwarz et al. [27] concluded that climate-related changes in sediment focusing have influenced the pattern of deposition on the OJP over the past ~ 200 ka.

To determine if the pattern of sediment focusing observed in Holocene sediments extends into the past on a regional scale, and to establish whether climate-related changes in sediment redistribution may have influenced the accumulation rates of ^3He and of other sedimentary constituents, two deep-sea cores were chosen for $x_s^{230}\text{Th}(o)$ profiling on the OJP: Site ODP806 ($0^\circ 19' \text{N}$, 159°E) and RC17-177 ($1^\circ 45' \text{N}$, 159°E ; Fig. 1). These cores were recovered from approximately the same water depth (2.5–2.6 km). Both of these cores have detailed oxygen isotope stratigraphies for the last ~ 250 ka and they have also been examined in detail to determine climate-

related changes in sediment composition and in CaCO_3 dissolution [20,22,24].

3. Methods

3.1. Uranium/thorium analyses

Concentrations of thorium and uranium isotopes were measured in 1-g aliquots of bulk sediment. The samples were analyzed at L-DEO by isotope-dilution inductively coupled plasma mass spectrometry (VG PlasmaQuad2 ICP-MS). Details of the chemical dissolution and separation methods, along with spike information, are provided in Higgins [19]. Initial excess ^{230}Th ($x_s^{230}\text{Th}(o)$) activities were calculated by decay-correcting $x_s^{230}\text{Th}$ using an independent chronology derived from the oxygen isotope stratigraphy of each core [22,28]. Total (measured) ^{230}Th activities were also corrected for both detrital ^{230}Th and ^{230}Th ingrowth from authigenic ura-

nium (~ 0.2 dpm g^{-1}). Detrital corrections (~ 0.1 dpm g^{-1}) were made using measured ^{232}Th concentrations and the known $^{230}\text{Th}/^{232}\text{Th}$ ratio in average shale [29]. These corrections are quite small and affect the final ^{230}Th values by $< 2\%$, so add negligible uncertainty to our overall reconstruction of $x_s^{230}\text{Th}$ accumulation. Analytical uncertainties for $x_s^{230}\text{Th}(\text{o})$ activities are less than $\pm 3\%$.

Approximately 25 discrete samples each were collected from cores ODP806 and RC17-177 to provide 7–10-ka resolution over the past 200 ka. At site RC17-177, the $\delta^{18}\text{O}$ age based model was taken from Le and Shackleton [22]. For ODP806, the samples were taken from Hole C, as samples from Hole B, used by Patterson and Farley, were no longer available in this portion of the core. The composite depth scale of Lyle et al. [30] allowed mapping of these samples back onto the depth scale of Hole B. However, little modification of the depth scale was necessary in these upper few meters of the record.

In addition, we measured $x_s^{230}\text{Th}(\text{o})$ in 10 samples from Site ODP806 Hole B covering the last 240 ka. K. Farley provided these samples as aliquots from the material used in the analysis of helium isotopes by Patterson and Farley [15]. Unlike the discrete samples described above, these samples were originally collected as homogenized composite samples, varying between 40 and 80 cm in length. These depth intervals were chosen to provide ~ 25 -ka (range 18–29 ka) coverage each, and generate an ‘average’ value for each interval. An average age was assigned to each of these samples at the approximate midpoint of each interval based on the orbitally tuned $\delta^{18}\text{O}$ age model of Berger et al. [15,28]. This model uses a template derived from a simple ice volume model and the primary Milankovitch frequencies. The only control points were known paleomagnetic and biostratigraphic datums over the last 2 Myr. Unlike RC17-177, this ‘quasi-continuous’ age model was not tuned to other records but to an orbital template model where sedimentation rates could be derived. These sedimentation rates averaged between 1.8 and 2.8 cm/ka throughout the record. Analytical uncertainties for ^3He analyses are $\sim 2\%$ and the average sample reproduc-

ibility for replicate ^3He measurements was estimated at ± 15 to 18% [15].

3.2. Excess thorium-derived mass accumulation rates

One strategy to correct for sediment redistribution when evaluating sediment mass accumulation rates (MAR) is to exploit the known rate of supply of ^{230}Th . The excess ^{230}Th -profiling method is based on the assumption that the regionally averaged rain rate of particulate ^{230}Th sinking to the seafloor (F_{Th}) is equivalent to the known rate of ^{230}Th production by ^{234}U decay in the overlying water column (P_{Th}) [31]. This is a reasonable assumption in that ^{230}Th is very particle reactive and, thus, has a short residence time ($= \sim 40$ years) in the water column [32]. Furthermore, this assumption has received substantial support from recent studies in which fluxes of particulate ^{230}Th have been evaluated using sediment traps [33,34]. Indeed, F_{Th} is estimated to be within 30% of P_{Th} over $\sim 70\%$ of the seafloor [35]. Because the residence time of dissolved U in the oceans is long (~ 400 ka; [36]), the production rate of ^{230}Th in seawater has remained virtually constant over the past few 10^5 years.

Consequently, the rain rates of any sedimentary component may be deduced as $F_i = C_i \cdot F_m$, or as:

$$F_i = \frac{C_i \cdot \beta \cdot z}{x_s^{230}\text{Th}(\text{o})} \quad (1)$$

where F_i is the flux of a given component ‘i’; C_i is the concentration of ‘i’ in a given sediment sample; $\beta \cdot z = P_{\text{Th}}$, where $\beta = 2.6 \times 10^{-5}$ dpm cm^{-3} ka^{-1} and z is depth of the water column in cm.

3.3. Focusing factors

Suman and Bacon [37] introduced the concept of a focusing factor (Ψ) to quantitatively describe the effect of lateral sediment redistribution on the measured accumulation rate of ^{230}Th in sediments. The sediment-focusing factor is defined as:

$$\Psi = \frac{\int_{t_2}^{t_1} [x_s^{230}\text{Th}(\text{o})] \cdot \rho_b \cdot dr}{P_{\text{Th}} \cdot (t_1 - t_2)}, \quad (2)$$

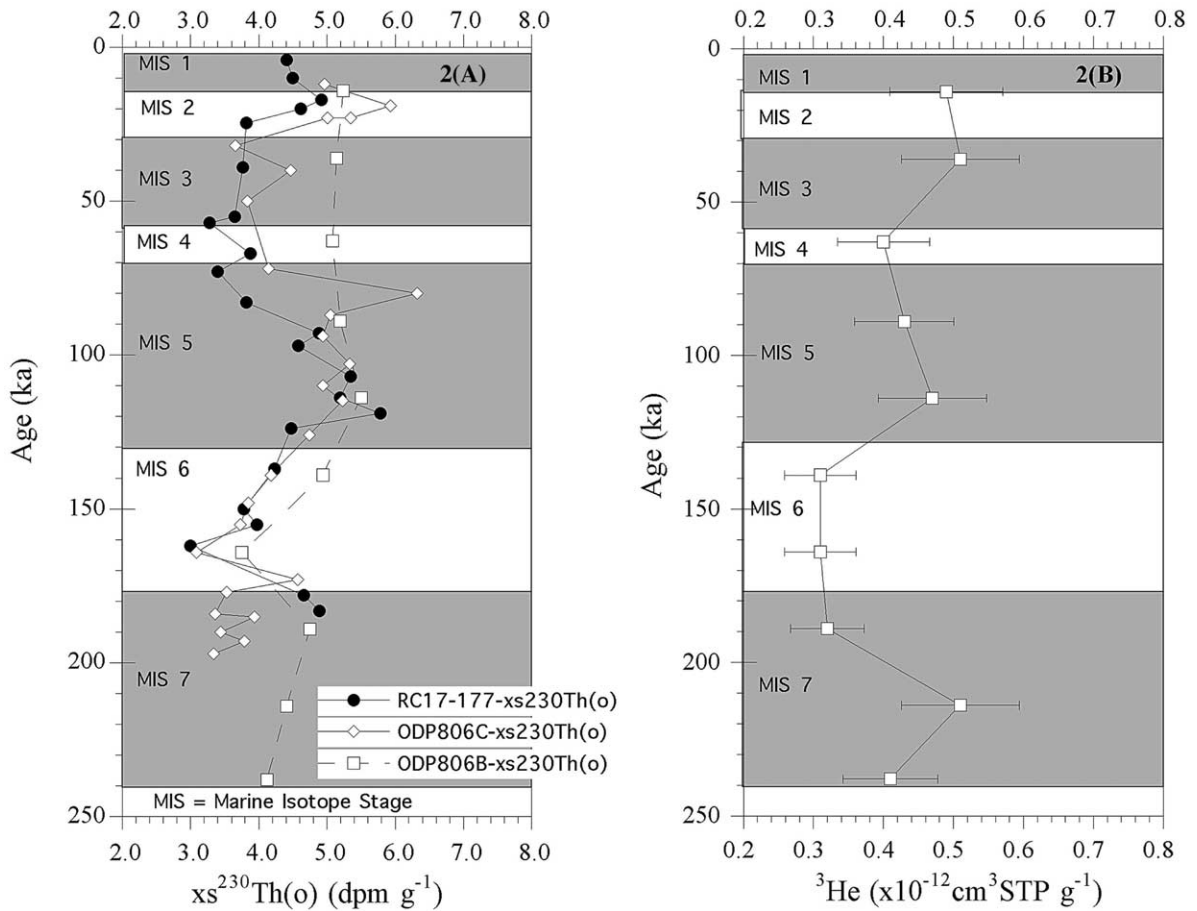


Fig. 2. (A) Concentrations of initial unsupported ^{230}Th plotted against age for RC17-177 and ODP806 (Hole C), determined by analyzing discrete samples, and for ODP806B, determined by analyzing homogenized composite samples covering intervals of 40–80 cm in length. The composite samples correspond to those analyzed for ^3He . (B) Concentrations of extraterrestrial ^3He in ODP806B determined by analyzing homogenized composite samples covering intervals of 40–80 cm in length. ^3He results from Patterson and Farley [15].

where r_i is the depth at interval i in the core, t_i is the age at depth i , $[x_s^{230}\text{Th}(o)]$ is the concentration of $x_s^{230}\text{Th}(o)$ in the sediment, P_{Th} is the production rate of ^{230}Th in the water column above the core site, and ρ_b is the bulk dry density of the sediment. A value of $\Psi > 1$ indicates sediment focusing to the site, whereas $\Psi < 1$ indicates net loss of sediment (winnowing) from the site. Evaluating Ψ provides a direct measure of climate-related changes in sediment redistribution by deep-sea currents. As can be seen in Eq. 2, errors in the sediment chronology propagate to errors in Ψ .

4. Results and discussion

The down-core pattern of $x_s^{230}\text{Th}(o)$ concentration in sediments from ODP806 is similar to that obtained from RC17-177 (Fig. 2a; Tables 1 and 2). However, the composite samples from ODP806B used previously for ^3He measurements [15] show a potential sampling bias in the upper portion of the record where the higher-resolution data from spot sampling ODP806C clearly document an interval (~ 30 – 60 ka) of lower $x_s^{230}\text{Th}(o)$ concentration (Fig. 2a). The remainder of the

Table 1
Radioisotopic data for ODP806C

Depth (cm)	Age ^a (kyr)	²³⁰ Th (dpm g)	1 S.D.	²³² Th (dpm g)	1 S.D.	²³⁸ U (dpm g)	1 S.D.	x _s ²³⁰ Th(o)	1 S.D.
30	12	4.50	0.10	0.052	0.003	0.200	0.01	4.96	0.17
48	19	5.14	0.11	0.205	0.010	0.214	0.03	5.93	0.21
55	23	4.46	0.04	0.171	0.007	0.172	0.01	5.35	0.15
55	23	4.20	0.23	0.193	0.008	0.209	0.01	5.01	0.22
77	32	2.62	0.04	0.194	0.008	0.156	0.01	3.66	0.13
100	40	3.27	0.01	0.154	0.006	0.306	0.02	4.47	0.11
120	50	2.73	0.05	0.137	0.005	0.614	0.03	3.83	0.13
162	72	2.28	0.02	0.115	0.007	0.209	0.01	4.14	0.14
180	80	3.16	0.06	0.142	0.006	0.153	0.01	6.32	0.22
192	87	2.58	0.04	0.154	0.006	0.447	0.02	5.05	0.18
205	94	2.25	0.02	0.126	0.005	0.227	0.02	4.94	0.12
227	103	2.24	0.06	0.152	0.006	0.219	0.01	5.33	0.19
240	110	2.02	0.06	0.113	0.010	0.285	0.01	4.94	0.17
250	115	2.06	0.03	0.119	0.005	0.305	0.02	5.23	0.21
270	126	1.88	0.03	0.164	0.007	0.487	0.02	4.74	0.17
281	139	1.71	0.04	0.166	0.007	0.653	0.03	4.18	0.19
298	148	1.51	0.08	0.144	0.006	0.10	0.03	3.85	0.13
311	155	1.76	0.04	0.222	0.009	1.002	0.05	3.73	0.18
329	164	1.57	0.03	0.168	0.007	1.006	0.06	3.09	0.11
348	173	3.03	0.03	0.124	0.005	2.373	0.12	4.57	0.16
355	177	2.03	0.03	0.211	0.011	0.571	0.03	3.53	0.12
370	184	0.86	0.01	0.139	0.006	0.256	0.01	3.36	0.09
372	185	1.36	0.03	0.195	0.009	0.697	0.03	3.94	0.14
385	190	0.92	0.02	0.142	0.006	0.341	0.02	3.44	0.12
390	193	0.94	0.02	0.133	0.005	0.317	0.02	3.79	0.13
400	197	0.77	0.03	0.106	0.004	0.240	0.01	3.34	0.08
400	197	0.88	0.03	0.106	0.006	0.427	0.02	2.98	0.16
415	202	0.85	0.02	0.145	0.006	0.460	0.02	2.70	0.12
420	205	0.88	0.01	0.133	0.005	0.356	0.02	3.60	0.21

^a Chronology is taken from Berger et al. [28]. Mapping of depths between Site ODP806 Holes B and C is taken from Lyle et al. [30], but little modification was required in the upper 4 m of the section. These discrete samples were collected over ~4-cm intervals. Depths shown mark midpoint of the sampled intervals.

Table 2
x_s²³⁰Th and ³He data for ODP806B

Samples	Average depth (cm)	Average age (ka)	³ He ^a		²³⁸ U		²³² Th		²³⁰ Th		x _s ²³⁰ Th(o)	
			(pcc STP g ⁻¹)	1 S.D.	(dpm g ⁻¹)	1 S.D.	(dpm g ⁻¹)	1 S.D.	(dpm g ⁻¹)	1 S.D.	(dpm g ⁻¹)	1 S.D.
Cycle 1 (9–51 cm)	30	14	0.49	0.08	0.16	0.003	0.12	0.002	4.70	0.141	5.24	0.14
Cycle 2 (51–101 cm)	75	36	0.51	0.08	0.15	0.003	0.15	0.003	3.88	0.128	5.14	0.21
Cycle 3 (101–161 cm)	130	63	0.40	0.07	0.36	0.007	0.15	0.007	3.08	0.092	5.08	0.18
Cycle 4 (161–211 cm)	185	89	0.43	0.07	0.32	0.006	0.13	0.003	2.51	0.075	5.19	0.23
Cycle 5 (211–260 cm)	235	114	0.47	0.08	0.20	0.004	0.12	0.002	2.10	0.042	5.50	0.19
Cycle 6 (260–311 cm)	285	139	0.31	0.05	0.38	0.008	0.14	0.004	1.70	0.102	4.94	0.17
Cycle 7 (311–361 cm)	335	164	0.31	0.05	0.96	0.023	0.15	0.003	2.23	0.067	3.75	0.13
Cycle 8 (361–416 cm)	387	189	0.32	0.05	0.66	0.013	0.16	0.003	1.44	0.043	4.75	0.11
Cycle 9 (416–471 cm)	443	214	0.51	0.08	0.29	0.011	0.12	0.006	0.89	0.035	4.41	0.15
Cycle 10 (471–520 cm)	495	238	0.41	0.07	0.31	0.006	0.12	0.007	0.76	0.038	4.12	0.22

^a ³He data, average ages, and depths from Patterson and Farley [15]

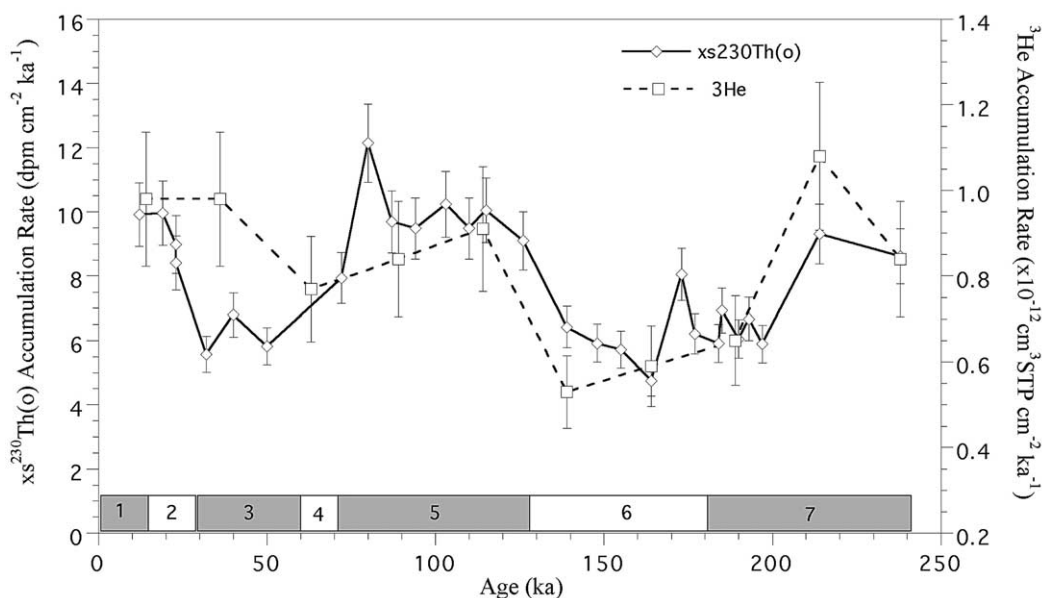


Fig. 3. Accumulation rates of initial unsupported ^{230}Th (discrete samples from Hole C) and ^3He (composite samples from Hole B) at ODP806. Accumulation rates of ^{230}Th and ^3He were calculated by multiplying measured concentrations by bulk sediment MARs (Fig. 4), which, in turn, were derived using the ^{18}O -based age model and measured *in situ* densities. Marine isotope stages (MISs) are indicated along the age axis.

Table 3
Radioisotope data for RC17-177

Depth (cm)	Age (ka)	^{232}Th (dpm g $^{-1}$)	1 S.D.	^{238}U (dpm g $^{-1}$)	1 S.D.	^{230}Th (dpm g $^{-1}$)	1 S.D.	$x_s^{230}\text{Th}(o)$ (dpm g $^{-1}$)	1 S.D.
5	4	0.10	0.004	0.21	0.004	4.32	0.01	4.41	0.12
14	10	0.12	0.004	0.21	0.004	4.20	0.06	4.50	0.17
26	17	0.15	0.006	0.15	0.003	4.32	0.08	4.92	0.20
37	20	0.20	0.007	0.15	0.006	3.99	0.03	4.62	0.18
53	24.5	0.12	0.003	0.23	0.005	3.17	0.09	3.82	0.15
65	39	0.15	0.006	0.25	0.005	2.78	0.02	3.77	0.08
77	55	0.11	0.004	0.19	0.004	2.33	0.06	3.65	0.15
85	57	0.14	0.004	0.22	0.004	2.10	0.01	3.28	0.13
95	67	0.16	0.007	0.24	0.005	2.27	0.09	3.88	0.16
104	73	0.10	0.003	0.22	0.004	1.89	0.01	3.40	0.10
114	83	0.12	0.004	0.22	0.004	1.94	0.03	3.82	0.15
124	93	0.14	0.003	0.17	0.003	2.21	0.05	4.88	0.20
133	97	0.09	0.005	0.19	0.004	2.02	0.14	4.58	0.18
143	107	0.14	0.004	0.13	0.002	2.12	0.24	5.35	0.21
153	114	0.10	0.003	0.16	0.003	1.95	0.05	5.19	0.21
162	119	0.10	0.004	0.17	0.004	2.07	0.07	5.78	0.23
173	124	0.10	0.003	0.11	0.002	1.53	0.01	4.48	0.18
184	137	0.15	0.006	0.17	0.003	1.35	0.04	4.23	0.18
195	150	0.12	0.003	0.15	0.003	1.08	0.05	3.78	0.15
203	155	0.19	0.005	0.09	0.002	1.05	0.01	3.97	0.16
213	162	0.13	0.004	0.18	0.004	0.84	0.02	3.00	0.12
223	178	0.14	0.006	0.18	0.002	0.81	0.09	4.66	0.19
234	183	0.13	0.004	0.20	0.004	0.78	0.06	4.89	0.20

Chronology from Le and Shackleton [22].

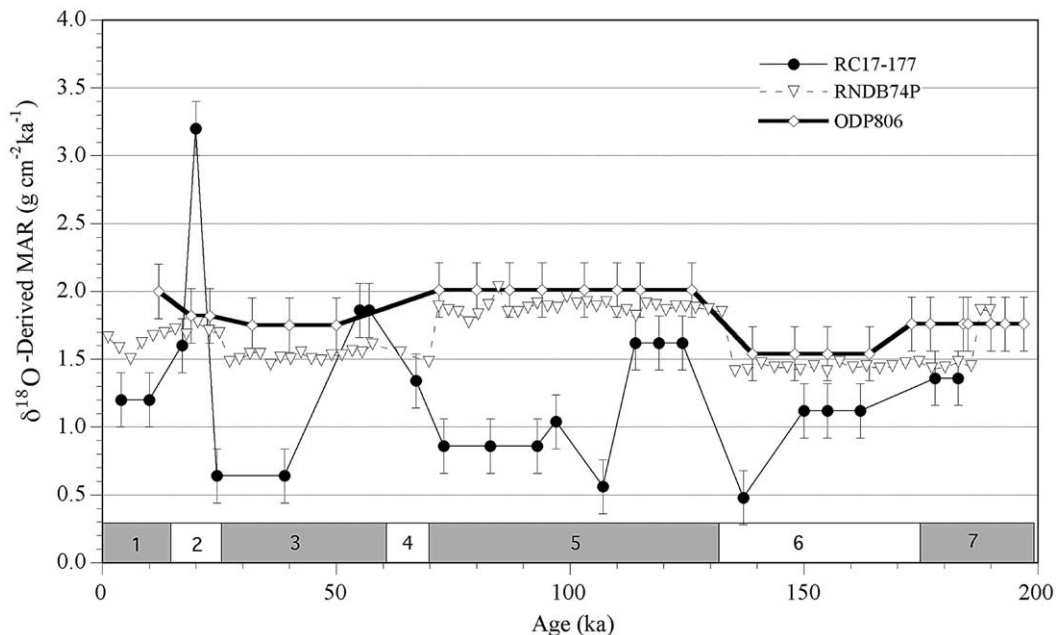


Fig. 4. MARs for core RC17-177 (1° 45'N), RNDB74P (equator) [22] and ODP806 (equator), calculated using the ^{18}O -based age model for each core and measured in situ densities. MISs are indicated along the age axis.

$x_s^{230}\text{Th}$ record from ODP806B agrees well with the other ODP806 data. The down-core pattern of ^3He concentration in sediments from ODP806B (Fig. 2b; results from [15]) is similar to that of $x_s^{230}\text{Th}(o)$ (Fig. 2a).

4.1. Nature and origin of the 100-ka cycle in ^3He accumulation

Accumulation rates of extraterrestrial ^3He at the location of ODP806 (Fig. 3) were evaluated by multiplying ^3He concentrations (Fig. 2b) by bulk sediment MAR estimates (Fig. 4) of Berger et al. [28]. The pattern of ^3He accumulation over the last 240 ka (Fig. 3) is representative of the longer records of Patterson and Farley [15] in that maximum ^3He accumulation rates occur during interglacial intervals and are, on average, 1.5–2 times greater than glacial values. Patterson and Farley [15] interpreted this pattern to reflect a 100-ka cycle in the accretion of IDPs.

Accumulation of $x_s^{230}\text{Th}(o)$ at the site of ODP806 also exhibits a 100-ka cycle in which the phase and amplitude are indistinguishable from those in the ^3He record (Fig. 3). A similar

100-ka cycle of ^{230}Th accumulation was reported by Schwarz et al. [27] following the study of core RNDB-74P, recovered from a site near that of ODP806 (Fig. 1). The similar characteristics of the ^{230}Th and ^3He records suggest that the 100-ka cycles apparent in each have a common source.

The amplitude (approximately a factor of 2) of the ~ 100 -ka cycle in ^{230}Th accumulation (Fig. 3) cannot be explained either by changes in its rate of production or by variability in the intensity of its scavenging by particles (see above). Therefore, we are left with two plausible interpretations of the 100-ka cycle in ^{230}Th accumulation: (1) Systematic errors in the chronology of the ODP806 record create an artificial 100-ka cycle (i.e. sediment MARs are biased by ascribing too much time to the glacial portion of each record and too little time to the interglacial portions); or (2) Sediment focusing leads to quasi-100-ka cycles in sediment deposition at this site. Whichever explanation is correct, the factor or process responsible for the 100-ka cycle in ^{230}Th accumulation must apply to ^3He as well. This means that the 100-ka cycle in the ^3He accumulation rate results either from an artifact in the inferred chronology,

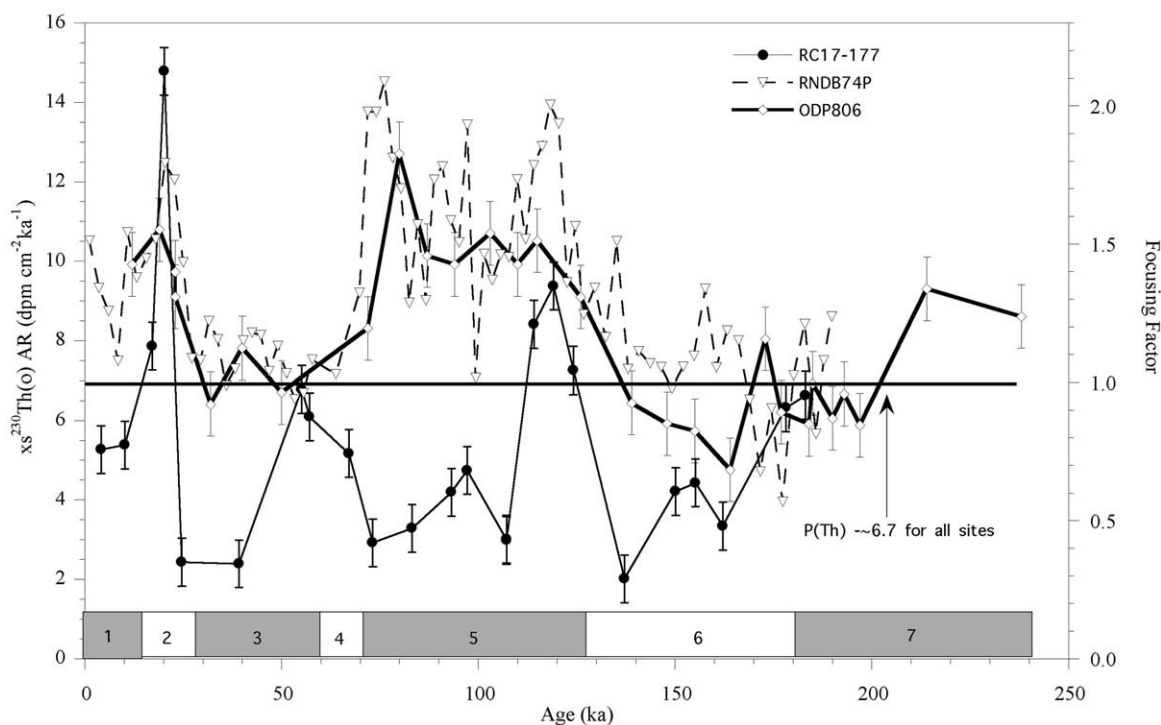


Fig. 5. Accumulation rates of initial unsupported ^{230}Th in cores RC17-177 ($1^\circ 45'\text{N}$), RNDB74P (equator) and ODP806 (equator) calculated by multiplying $x_s^{230}\text{Th}(o)$ concentrations by bulk sediment MARs (Fig. 4). The production rate of ^{230}Th in the water column at these sites, which have a similar water depth, is $\sim 6.7 \text{ dpm cm}^{-2} \text{ ka}^{-1}$. The accumulation rate of ^{230}Th is also expressed in terms of the focusing factor (Eq. 2) to illustrate quantitatively the relative net gain (focusing) or loss (winnowing) of sediment. Marine isotope stages are indicated along the age axis.

or from sediment focusing, but cannot be ascribed to regular changes in the supply of IDPs from space.

4.2. Evidence for sediment redistribution

Accumulation rates of ^{230}Th provide a robust indicator of sediment redistribution. The integrated rate of production of ^{230}Th in the water column depends only on water depth. The depths of ODP806 and RNDB-74P on the equator (2521 m and 2547 m, respectively) are nearly the same as that at the site of RC17-177 at $\sim 2^\circ\text{N}$ (2605 m). At this depth, the production rate of ^{230}Th is $\sim 6.7 \text{ dpm cm}^{-2} \text{ ka}^{-1}$. Because the flux of particulate ^{230}Th from the water column nearly everywhere is close to its integrated production rate (see above), the accumulation rate of ^{230}Th

in sediments at these sites is expected to be $\sim 6.7 \text{ dpm cm}^{-2} \text{ ka}^{-1}$.

Accumulation rates of ^{230}Th in these cores, evaluated by multiplying $x_s^{230}\text{Th}(o)$ by the bulk sediment MAR, depart substantially from the expected value. Expressed in terms of the focusing factor (Eq. 2), Ψ varies between ~ 1 during glacial to as much as 2 during interglacials at the sites on the equator (Fig. 5). At 2°N , the pattern is more variable, but Ψ is generally < 1 and often as low as ~ 0.5 (Fig. 5). Because departures of the ^{230}Th accumulation rate by as much as a factor of two from its production rate cannot be attributed to changes in production or scavenging of ^{230}Th , these features are most reasonably ascribed to sediment redistribution.

While the 100-ka cycles in ^{230}Th MAR may still be attributed to systematic errors in the interpre-

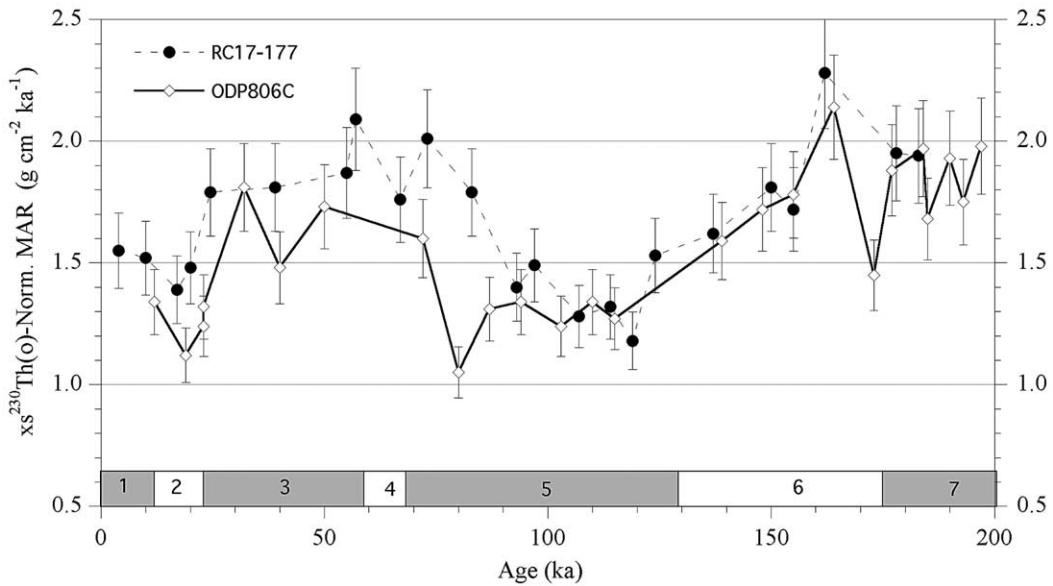


Fig. 6. Sediment MARs calculated by normalizing to ^{230}Th (Eq. 1) for cores RC17-177 ($1^{\circ}45'\text{N}$) and ODP806 (equator). Marine isotope stage boundaries are shown along the age axis.

tation of the $\delta^{18}\text{O}$ stratigraphy, the overall net gain of sediment at the equator and net loss at 2°N is a robust conclusion that is reached without relying on the detailed age model of any core. The boundary between Marine isotope stage (MIS) 7 and MIS6 is clearly distinguished in the $\delta^{18}\text{O}$ record of each core. Consequently, the relative uncertainty in the age assigned to the MIS7/MIS6 boundary is small compared to its absolute age, thereby allowing precise evaluation of the expected inventory of $x\text{s}^{230}\text{Th}(\text{o})$ integrated from the core top down to this boundary. Compared to the expected inventory, we find a deficit of $\sim 30\%$ at 2°N , and an excess of $\sim 35\%$ at the equator (ODP806). To account for these imbalances between production and accumulation of ^{230}Th , there must have been a net loss of sediment at 2°N and a net gain of sediment at the equator due to sediment redistribution over the past ~ 185 ka.

4.3. Comparison to regional productivity patterns

Comparing sediment MARs to regional patterns of primary production provides further evidence for sediment redistribution. Sediment

MARs derived using $\delta^{18}\text{O}$ age models are, on average, much lower at 2°N than at the equator (Fig. 4). When sediment MARs are corrected for sediment focusing by normalizing to $x\text{s}^{230}\text{Th}(\text{o})$ (Eq. 1), however, the resulting $x\text{s}^{230}\text{Th}(\text{o})$ -normalized MARs at the equator are indistinguishable from those at 2°N (Fig. 6).

Unlike the central and eastern equatorial Pacific Ocean, where equatorial upwelling creates strong maxima in biological productivity and in sediment accumulation at the equator [38], the absence of strong upwelling over the OJP results in little meridional variability in primary productivity between 5°N and 5°S [39]. Given that OJP sediments are $> 90\%$ biogenic, the spatial pattern of sediment MAR is expected to reflect the regional pattern of primary production. Consequently, the sediment MARs calculated by normalizing to $x\text{s}^{230}\text{Th}(\text{o})$ (i.e. corrected for sediment focusing), which show little difference between the equator and 2°N (Fig. 6), are more consistent with regional productivity patterns than are MARs derived from the $\delta^{18}\text{O}$ age models (Fig. 4), supporting our hypothesis that the $\delta^{18}\text{O}$ -derived MARs have been influenced by sediment redistribution.

4.4. CaCO_3 cycles

Comparing the $\delta^{18}\text{O}$ -derived MAR records from the OJP with those expected, considering the well-established CaCO_3 dissolution cycles in the Pacific Ocean, provides further evidence for sediment focusing. Maximum CaCO_3 dissolution in Pacific sediments occurs during interglacials, whereas maximum preservation occurs during glacials, although maximum dissolution lags behind the minimum in global ice volume by roughly 10 ka [40]. Le and Shackleton [22] showed that this Pacific pattern of CaCO_3 dissolution is evident in OJP sediments to water depths as shallow as ~ 1.5 km. Therefore, if other factors were held constant, then we would expect to find minimum rates of CaCO_3 accumulation during interglacial periods.

Before comparing expected patterns of CaCO_3 accumulation with those observed, we first consider the possibility that other factors were not held constant. The accumulation rate of CaCO_3 is dependent on its rate of production in surface waters as well as its rate of dissolution on the sea floor. While there is no known sedimentary proxy for CaCO_3 production, by measuring the ^{230}Th -normalized rate of excess Ba accumulation in RNDB-74P, Schwarz et al. [27] showed that the export flux of organic carbon in the OJP region has remained relatively constant over the past ~ 200 ka. Although CaCO_3 production need not scale linearly with organic carbon flux, there is no reason to expect large variability in CaCO_3 production if organic carbon flux has remained relatively constant. Therefore, the accumulation rate of CaCO_3 in OJP sediments should reflect more strongly past changes in preservation of CaCO_3 than changes in its rate of production. Consequently, we expect the pattern of CaCO_3 accumulation in OJP sediments to exhibit minima during interglacials and maxima during glacial periods.

Changes in bulk sediment MAR provide a good representation of changes in CaCO_3 accumulation on the OJP at the depths of the cores studied here because these sediments have CaCO_3 contents generally $\geq 90\%$ [20]. In cores recovered from the equator, sediment MARs derived from

$\delta^{18}\text{O}$ stratigraphy exhibit maxima during interglacials and minima during glacials (Fig. 4), whereas the inverse pattern is observed in ^{230}Th -normalized MARs (Fig. 6). The ^{230}Th -normalized MARs are consistent with the Pacific pattern of CaCO_3 dissolution [22,40], whereas the $\delta^{18}\text{O}$ -derived sediment MARs are not. Accepting that the $\delta^{18}\text{O}$ -derived chronologies are reliable at the resolution of 100-ka glacial–interglacial cycles, the anti-phased relationship between $\delta^{18}\text{O}$ -derived MARs and the Pacific pattern of CaCO_3 dissolution indicates that the 100-ka cycles in $\delta^{18}\text{O}$ -derived MAR must have been generated by sediment redistribution. Otherwise, it would be impossible to explain the observation that maximum sediment MAR coincides with periods of maximum CaCO_3 dissolution.

4.5. Processes influencing sediment redistribution

Although the processes regulating sediment redistribution on the OJP remain unknown, a few important diagnostic patterns provide clues to guide future research on this question. Records presented here, covering the past ~ 200 ka, are consistent with the results from a much larger number of OJP cores showing a systematic pattern during the Holocene of enhanced sediment deposition at the equator compared to sites off the equator [25]. Preferential deposition of sediment at the equator has been a consistent feature of this region for at least the last two complete glacial cycles, and possibly longer.

Although there is net winnowing and loss of sediment from the 2°N site (see above), the temporal pattern of $\delta^{18}\text{O}$ -derived MAR at 2°N is unrelated to that at the equator (Fig. 4), indicating that the 2°N site has not served as the primary source of sediment transported to the equator. Down-slope (Fig. 1) sediment transport processes may be involved instead.

Whatever the actual physical transport mechanism, it has produced similar 100-ka cycles in the accumulation rates of excess Ba [27], of $x\text{s}^{230}\text{Th}(\text{o})$ and ^3He (IDPs; Fig. 3), and of bulk sediment (Fig. 4). The processes regulating the 100-ka cycles in sediment redistribution must, therefore,

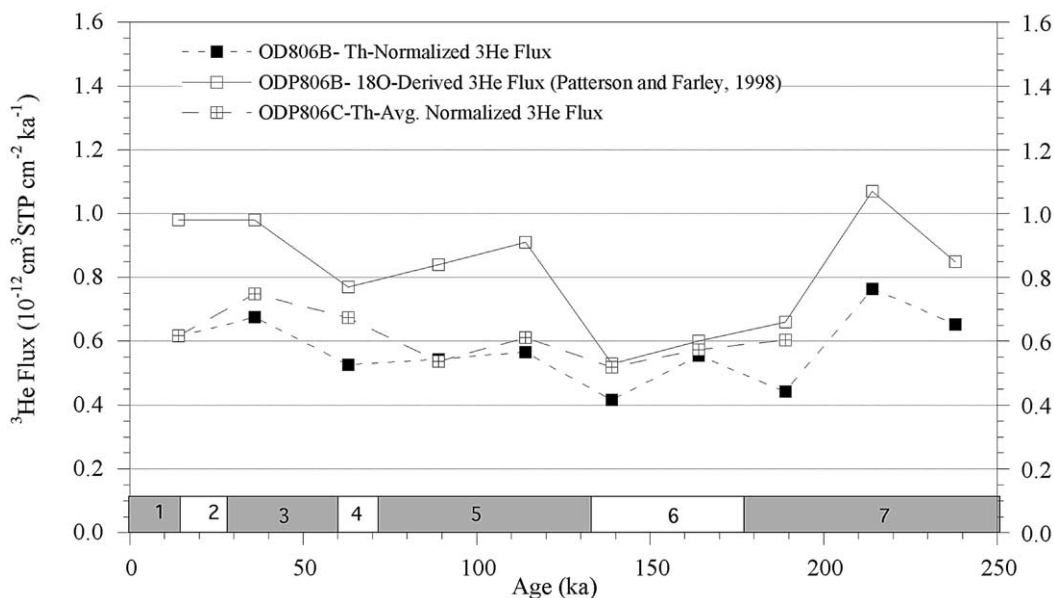


Fig. 7. Accumulation rates of ^3He were estimated by three methods. In open squares are accumulation rates derived originally by Patterson and Farley [15] by multiplying ^3He concentrations by ^{18}O -based sediment MARs (Fig. 4). In solid squares are accumulation rates derived by multiplying ^3He concentrations by ^{230}Th -normalized MARs using ^{230}Th data from the composite samples of ODP806B analyzed for ^3He . In the cross-hatched squares are Th-normalized ^3He fluxes determined by averaging $x_s^{230}\text{Th}(o)$ data in the higher-resolution dataset from ODP806C and binning them into age intervals equivalent to those of the composite samples of Patterson and Farley [15].

act without composition-dependent fractionation of sedimentary constituents, a conclusion that is consistent with the results of earlier studies [29]. Furthermore, periods of maximum sediment focusing (interglacials) coincide with periods of maximum CaCO_3 dissolution that is attributable, at least in part, to changes in deep-water composition [22]. A similar correlation was found in central equatorial Pacific sediments [17,18], indicating that sediment focusing and CaCO_3 dissolution must reflect a common response to climate-related change in deep-sea circulation. Details concerning the nature and origin of climate-related changes in deep-water chemistry and circulation remain to be established.

4.6. Fluxes of ^3He in a global context

Having established that the accumulation of sediment at the OJP sites is influenced by climate-related changes in sediment redistribution, we now re-examine the record of ^3He accumu-

lation by normalizing to $x_s^{230}\text{Th}(o)$ to correct for sediment focusing. Normalizing to $x_s^{230}\text{Th}(o)$ reduces, and nearly eliminates, the 100-ka cycle in ^3He accumulation over the past 240 ka that was evident in the original ODP806 record obtained using $\delta^{18}\text{O}$ -derived sediment MARs (Fig. 7). The average ^{230}Th -normalized ^3He flux is $0.60 \pm 0.11 \times 10^{-12} \text{ cm}^3 \text{ STP cm}^{-2} \text{ ka}^{-1}$, which compares favorably with the corresponding average ^{230}Th -normalized ^3He flux to central equatorial Pacific sediments ($0.78 \pm 0.20 \times 10^{-12} \text{ cm}^3 \text{ STP cm}^{-2} \text{ ka}^{-1}$) reported by Marcantonio et al. [17,18], with the global average Holocene ^{230}Th -normalized ^3He flux (0.77 ± 0.2) compiled from 17 sites by Higgins [19], and with ^3He fluxes from ice cores in Greenland and Antarctica (Greenland: 0.62 ± 27 ; Vostok: 0.77 ± 0.25 ; [41]). These results indicate that the accretion of IDPs is relatively uniform globally. Furthermore, in none of the records with duration > 100 ka has there been found a 100-ka cycle in ^{230}Th -normalized ^3He flux [19]. Therefore, we conclude that the 100-ka cycle in ^3He accumu-

lation described in previous studies [13,15] reflects climate-related changes in sediment redistribution rather than cyclical changes in IDP accretion.

5. Summary

Sediment accumulation rates on the OJP derived using $\delta^{18}\text{O}$ stratigraphies reveal ~ 100 -ka cycles with maximum mass (primarily CaCO_3) accumulation occurring during interglacial periods. Driven by the bulk sediment mass accumulation record, similar 100-ka cycles in accumulation of ^3He , ^{230}Th , and excess Ba are derived as well. Several lines of reasoning suggest that this temporal pattern of sediment accumulation reflects climate-related changes in sediment redistribution rather than changes in the supply of bulk sediment or of the individual constituents. The accumulation rate of ^{230}Th in these sediments deviates from its production rate in the overlying water column by more than can be ascribed to variability in scavenging intensity, indicating that sediment redistribution has influenced the accumulation of ^{230}Th . Co-variability in the supply of extraterrestrial ^3He , authigenic ^{230}Th , and biogenic xsBa is not expected a priori. The observed 100-ka cycle in the accumulation of these constituents is more readily explained in terms of variable sediment redistribution superimposed on a relatively constant supply of each tracer than by the unlikely coincidence that the supply of each of these tracers, which have very different sources, has varied through time.

The average focusing-corrected (^{230}Th -normalized) flux of ^3He to OJP sediments over the past 240 ka is $0.60 \pm 0.11 \times 10^{-12} \text{ cm}^3 \text{ STP cm}^{-2} \text{ ka}^{-1}$, which is similar to fluxes determined for other regions in marine sediments and in polar ice cores. Normalizing to xs $^{230}\text{Th}(o)$ eliminates the apparent 100-ka cycle in ^3He accumulation in OJP sediments, as it does at other sites where this strategy has been applied. Consequently, we conclude that the accretion of IDPs has remained relatively constant (within analytical uncertainty) and has not varied detectably over the past ~ 240 ka. These results fail to support the hypothesis linking the 100-ka cycle of ice ages to changes

in the angle of Earth's orbital inclination, but they hold promise for the use of ^3He as a constant-flux proxy for paleoceanographic studies.

Acknowledgements

This project was supported by NSF collaborative research grants to R.F.A. and M.S. (OCE 97-11870) and F.M. (OCE 97-14898). The LDEO Deep-Sea Sample Repository (RC17–177 samples) is supported by grants from NSF (Grant #OCE0002380) and ONR (Grant #N00014-02-1-0073). K. Farley and the Ocean Drilling Program core repository provided samples for Site ODP-806. S.M.H. received support from a NASA Global Change Fellowship (NGT5-30016). We thank A. Mix, A. Mangini, M. Christl, and an anonymous reviewer for their comments. This is L-DEO Contribution No. 6359. [**BARD**]

References

- [1] J.D. Hays, J. Imbrie, N.J. Shackleton, Variations in the Earth's orbit: pacemaker of the ice ages, *Science* 194 (1976) 1121–1132.
- [2] J. Imbrie, E.A. Boyle, S.C. Clemens, A. Duffy, W.R. Howard, G. Kukla, J. Kutzbach, D.G. Martinson, A. McIntyre, A.C. Mix, B. Molino, J.J. Morley, L.C. Peterson, N.G. Pisias, W.L. Prell, M.E. Raymo, N.J. Shackleton, J.R. Toggweiler, On the structure and origin of major glaciation cycles. 1. Linear responses to Milankovitch forcing, *Paleoceanography* 7 (1992) 701–738.
- [3] D.G. Martinson, N.G. Pisias, J.D. Hays, J. Imbrie, T.C. Moore Jr., N.J. Shackleton, Age dating and the orbital theory of the Ice Ages: development of a high-resolution 0 to 300 000-year chronostratigraphy, *Quat. Res.* 27 (1987) 1–30.
- [4] N.J. Shackleton, The oxygen isotope stratigraphic record of the Late Pleistocene, *Phil. Trans. R. Soc. London Ser. B.* 280 (1977) 169–182.
- [5] J. Imbrie, A. Berger, E.A. Boyle, S.C. Clemens, A. Duffy, W.R. Howard, G. Kukla, J. Kutzbach, D.G. Martinson, A. McIntyre, A.C. Mix, B. Molino, J.J. Morley, L.C. Peterson, N.G. Pisias, W.L. Prell, M.E. Raymo, N.J. Shackleton, J.R. Toggweiler, On the structure and origin of major glaciation cycles. 2. The 100 000-year cycle, *Paleoceanography* 8 (1993) 698–735.
- [6] Imbrie, J., Hays, J.D., Martinson, D.G., McIntyre, A., Mix, A.C., Morley, J.J., Pisias, N.G., Prell, W.L., Shackleton, N.J., 1984. The orbital theory of Pleistocene climate: support from a revised chronology of the marine

- ¹⁸O record. In: Berger, A.L., (Ed.), *Milankovitch and Climate: Part 1*. D. Reidel, Amsterdam, pp. 269–305.
- [7] R.A. Muller, G.J. MacDonald, Glacial cycles and orbital inclination, *Nature* 377 (1995) 107–108.
- [8] R.A. Muller, G.J. MacDonald, Simultaneous presence of orbital inclination and eccentricity in proxy climate records from Ocean Drilling Program Site 806, *Geology* 25 (1997) 3–6.
- [9] Dermott, S.F., Grogan, K., Gustafson, B.A.S., Jayaraman, S., Kortenkamp, S.J., Xu, Y.L., 1996. Sources of interplanetary dust. In: Gustafson, B.A.S., Hanner, M.S. (Eds.), *Physics, Chemistry, and Dynamics of Interplanetary Dust*. ASP, Houston, p. 143–153.
- [10] S.J. Kortenkamp, S.F. Dermott, A 100 000-year periodicity in the accretion rate of interplanetary dust, *Science* 280 (1998) 874–876.
- [11] S.G. Love, D.E. Brownlee, A direct measurement of the terrestrial mass accretion rate of cosmic dust, *Science* 262 (1991) 550–553.
- [12] P. Fraundorf, The distribution of temperature maxima for micrometeorites decelerated in the Earth's atmosphere without melting, *J. of Geophys. Res.* 7 (1980) 765–768.
- [13] K.A. Farley, D.B. Patterson, A 100-kyr periodicity in the flux of extraterrestrial ³He to the sea floor, *Nature* 378 (1995) 600–603.
- [14] F. Marcantonio, S.M. Higgins, R.F. Anderson, M. Stute, P. Schlosser, E.T. Rasbury, Terrestrial helium in deep sea sediments, *Geochim. Cosmochim. Acta* 62 (1998) 1535–1543.
- [15] D.B. Patterson, K.A. Farley, Extraterrestrial ³He in sea-floor sediments Evidence for correlated 100 kyr periodicity in the accretion rate of interplanetary dust, orbital parameters, and Quaternary climate, *Geochim. Cosmochim. Acta* 62 (1998) 3669–3882.
- [16] F. Marcantonio, R.F. Anderson, S.M. Higgins, M. Stute, P. Schlosser, Sediment focusing in the central equatorial Pacific Ocean, *Paleoceanography* 16 (2001) 260–267.
- [17] F. Marcantonio, R.F. Anderson, M. Stute, N. Kumar, P. Schlosser, A. Mix, Extraterrestrial ³He as a tracer of marine sediment transport and accumulation, *Nature* 383 (1996) 705–707.
- [18] F. Marcantonio, N. Kumar, M. Stute, R.F. Anderson, M.A. Seidl, P. Schlosser, A. Mix, A comparative study of accumulation rates derived by He and Th isotope analysis of marine sediments, *Earth Planet. Sci. Lett.* 133 (1995) 549–555.
- [19] Higgins, S.M., 2001. *Extraterrestrial Tracer in the Sea: Evaluation and Application of ³He in Interplanetary Dust Particles as a Constant Flux Tracer in Marine Sediments*. Ph.D. thesis, Columbia University, New York, 203 pp.
- [20] W.H. Berger, L.W. Kroenke, L.A. Mayer, J. Backman, T.R. Janecek, L. Krissek, M. Leckie, M.W. Lyle, The record of Ontong Java Plateau: main results of ODP Leg 130, *GSA Bull.* 104 (1992) 954–972.
- [21] J.C. Herguera, W.H. Berger, Glacial to postglacial drop in productivity in the western equatorial Pacific: mixing rate vs. nutrient concentrations, *Geology* 22 (1994) 629–632.
- [22] J. Le, N.J. Shackleton, Carbonate dissolution fluctuations in the western equatorial Pacific during the late Quaternary, *Paleoceanography* 7 (1992) 21–42.
- [23] N.J. Shackleton, N.D. Opdyke, Oxygen isotope and paleomagnetic stratigraphy of equatorial Pacific core V28-238 oxygen isotope temperatures and ice volumes on a 10 000 and 100 000 year time scale, *Quat. Res.* 3 (1973) 39–55.
- [24] G. Wu, W.H. Berger, Pleistocene d¹⁸O records from the Ontong Java Plateau: effects of winnowing and dissolution, *Mar. Geol.* 96 (1991) 193–209.
- [25] W.S. Broecker, E. Clark, D.C. McCorkle, I. Hajdas, G. Bonani, Core top ¹⁴C ages as a function of latitude and water depth on the Ontong Java Plateau, *Paleoceanography* 14 (1999) 13–22.
- [26] S.M. Higgins, W.S. Broecker, R.F. Anderson, D.C. McCorkle, D. Timothy, Enhanced sedimentation along the equator in the western Pacific, *Geophys. Res. Lett.* 26 (1999) 3489–3492.
- [27] B. Schwarz, A. Mangini, M. Segl, Geochemistry of a piston core from Ontong Java Plateau (western equatorial Pacific): evidence for sediment redistribution and changes in paleoproductivity, *Geol. Rundsch.* 85 (1996) 536–545.
- [28] W.H. Berger, M.K. Yasuda, T. Bickert, G. Wefer, T. Takayama, Quaternary time scale for the Ontong Java Plateau: Milankovitch template for the Ocean Drilling Program Site 806, *Geology* 22 (1994) 463–487.
- [29] Taylor, S.R., McLennan, S.M., 1985. *The Continental Crust: Its Composition and Evolution*. Blackwell Scientific Publications, 185 pp.
- [30] Lyle, M., Wilkens, R.H., Mayer, L.A., 1993. Detailed stratigraphic correlation of the Neogene sedimentary sequences on the Ontong Java Plateau by well logging, ODP Sites 803, 805, 806, 807, and DSDP Site 586. In: Berger, W.H., Kroenke, L.W., Mayer, L.A. (Eds.), *Proc. ODP Sci. Results* 130, pp. 587–606.
- [31] R. Francois, M.P. Bacon, D.O. Suman, ²³⁰Th Profiling in deep-sea sediments high resolution records of flux and dissolution of carbonate in the equatorial Atlantic during the last 24 000 yrs, *Paleoceanography* 5 (1990) 761–787.
- [32] R.F. Anderson, M.P. Bacon, P.G. Brewer, Removal of ²³⁰Th and ²³¹Pa at ocean margins, *Earth Planet. Sci. Lett.* 66 (1983) 73–90.
- [33] E.F. Yu, R. Francois, M.P.S. Bacon, S. Honjo, A.P. Fleer, S.J. Manganini, M.M.R. van der Loeff, V. Ittekkot, Trapping efficiency of bottom-tethered sediment traps estimated from the intercepted fluxes of Th-230 and Pa-231, *Deep-Sea Res.* I 48 (2001) 865–889.
- [34] J.C. Scholten, J. Fietzke, S. Vogler, M.M.R. van der Loeff, A. Mangini, W. Koeve, J. Waniek, P. Stoffers, J. Kuss, S. Neuer, Trapping efficiencies of sediment traps from the deep eastern North Atlantic: the ²³⁰Th calibration, *Deep-Sea Res.* II 48 (2001) 2343–2408.
- [35] G.M. Henderson, C. Heinze, R.F. Anderson, A.M.E. Winguth, Global distribution of the ²³⁰Th flux to ocean

- sediments constrained by GCM modelling, *Deep-Sea Res.* 46 (1999) 1861–1893.
- [36] A. Mangini, C. Sonntag, G. Bertsch, E. Muller, Evidence for a higher natural U content in world rivers, *Nature* 278 (1979) 337–339.
- [37] D.O. Suman, M.P. Bacon, Variations in Holocene sedimentation in the North American Basin determined by ^{230}Th measurements, *Deep-Sea Res.* 36 (1989) 869–878.
- [38] R.W. Murray, M. Leinen, A.R. Isern, Biogenic flux of Al to sediment in the central equatorial Pacific Ocean: evidence for increased productivity during glacial periods, *Paleoceanography* 8 (1993) 651–670.
- [39] D.J. Mackey, J.S. Parslow, F.B. Griffiths, H.W. Higgins, B. Tilbrook, Phytoplankton productivity and the carbon cycle in the western Equatorial Pacific under El Niño and non-El Niño conditions, *Deep-Sea Res. II* 44 (1997) 1951–1978.
- [40] J.W. Farrell, W.L. Prell, Climatic change and CaCO_3 preservation: an 800 000 year bathymetric reconstruction from the central equatorial Pacific ocean, *Paleoceanography* 4 (1989) 447–466.
- [41] E.J. Brook, M. Kurz, J. Curtice, S. Cowburn, Accretion of interplanetary dust in Polar ice, *Geophys. Res. Lett.* 27 (2000) 3145–3148.